Alexandria Engineering Journal (2016) 55, 2309–2320

HOSTED BY

Alexandria University

Alexandria Engineering Journal

www.elsevier.com/locate/aej
www.sciencedirect.com

ORIGINAL ARTICLE

# Numerical modelling of unsteady flow behaviour in the rectangular jets with oblique opening

James T. Hart [a], Md. Rezwanul Karim [a,b], Arafat A. Bhuiyan [a,b], Peter Witt [c], Jamal Naser [a,*]

[a] Faculty of Science, Engineering and Technology, Swinburne University of Technology, Hawthorn, VIC 3122, Australia
[b] Department of Mechanical and Chemical Engineering, Islamic University of Technology (IUT), Gazipur 1704, Dhaka, Bangladesh
[c] CSIRO, Division of Minerals, Clayton, VIC 3168, Australia

Received 21 January 2016; revised 2 May 2016; accepted 11 May 2016
Available online 2 June 2016

KEYWORDS

Recessed slot-burner;
Tangentially fired boiler;
Rectangular jet;
Transient

**Abstract** Vortex shedding in a bank of three rectangular burner-jets was investigated using a CFD model. The jets were angled to the wall and the whole burner was recessed into a cavity in the wall; the ratio of velocities between the jets varied from 1 to 3. The model was validated against experimentally measured velocity profiles and wall pressure tapings from a physical model of the same burner geometry, and was generally found to reproduce the mean flow field faithfully. The CFD model showed that vortex shedding was induced by a combination of an adverse pressure gradient, resulting from the diffuser-like geometry of the recess, and the entrainment of fluid into the spaces separating the jets. The asymmetry of the burner, a consequence of being angled to the wall, introduced a cross-stream component into the adverse pressure gradient that forced the jets to bend away from their geometric axes, the extent of which depended upon the jet velocity. The vortex shedding was also found to occur in different jets depending on the jet velocity ratio.


## 1. Introduction

Stable combustion in a tangentially-fired boiler is achieved by orienting the burner jets so as to induce a swirling vortex in the central region of the boiler, providing enhanced mixing and extending the residence time of the fuel to ensure complete burnout. A burner set may contain several burners located in a vertical plane, with a single burner consisting of a primary fuel/air nozzle, sandwiched between secondary air nozzles above and below. The nozzles are rectangular and there is significant separation between them.

In gas fired and black-coal fired boilers the flames are anchored to the nozzle and most of the combustion occurs in the near field of the burner-jets [1–4]. In the near-field of burner jets in a tangentially fired lignite boiler the lignite particles undergo pyrolysis and volatile matter is driven from the particle, but only a limited amount of combustion occurs; therefore, turbulent mixing in the near-field is less crucial. The main aims were to heat the lignite and air by mixing with entrained hot furnace gases and to deliver it to the correct location in the centre of the furnace. Near-field aerodynamics is still important for entrainment and for ensuring that the jets

* Corresponding author.
E-mail address: jnaser@swin.edu.au (J. Naser).
Peer review under responsibility of Faculty of Engineering, Alexandria University.

http://dx.doi.org/10.1016/j.aej.2016.05.008

reach the centre of the furnace at the correct location and with sufficient momentum for generating the required swirl.

Stage II boilers of the Yallourn W power station in the Latrobe Valley, Australia, feature burner nozzles that are recessed in the boiler walls, which permit the boiler size to be reduced while maintaining the correct flame length. Upon commissioning, this burner design was found to operate in a highly unsteady, unpredictable and unsatisfactory manner, impacting significantly on furnace performance. Under certain operating conditions the fuel jets were found to turn so far away from their intended trajectories that they even impinged on the walls adjacent to the burner, causing excessive fouling. This burner design is the object of the current study.

The level of combustion in the near field is low enough that aerodynamics are sufficiently decoupled from the effects of intense chemical reaction and radiative heat transfer, which would otherwise alter the physical properties of the flow. Therefore, isothermal modelling can reasonably be expected to give a good indication how the jets from different burner geometries deliver the fuel stream and mix it with the surrounding gases within the furnace.

Previous investigations by the boiler operator [5,6] in which isothermal, scaled-down physical models were made of several burner geometries, provided measurements of velocity made with a Pitot tube and measurements of the static pressure on the recess walls. Three-dimensional effects are very important in such complex flows, and if modelled correctly, the full flow field prediction from a computational fluid dynamics (CFD) model can provide more insight into the burner aerodynamics than physical modelling alone. The aim of this research was to develop a good understanding of the complex flow patterns that were developed as a result of recessing the burner nozzles in the furnace wall. This paper highlights the unsteady modes of the jets peculiar to this burner configuration and uncovers the cause of the unsteadiness. This knowledge will be valuable in developing future designs and in modifying existing ones.

## 2. Numerical models and procedures used

The CFD code CFX was used to model the fluid flow, which was subsonic, isothermal, single phase and fully turbulent. The resulting simplified Reynolds Averaged Navier–Stokes (RANS) system of equations solved in this numerical model was for a constant density, constant temperature and transient flow:

$$\partial\rho/\partial t + \nabla.(\mathbf{U}) = 0, \tag{1}$$

$$\partial\rho\mathbf{U}/\partial t + \nabla\cdot(\rho\mathbf{U}\otimes\mathbf{U}) = \nabla\cdot(\sigma - \rho\overline{\mathbf{u}\otimes\mathbf{u}}), \tag{2}$$

where $\sigma$ is the stress tensor

$$\sigma = -p\delta + \mu(\nabla\mathbf{U} + (\nabla\mathbf{U})^{\mathrm{T}}). \tag{3}$$

Here $\rho$ is the fluid density, $\mathbf{U} = (U, V, W)$ is the mean velocity vector, $p$ is the pressure, $\mu$ is the molecular viscosity and $\rho\overline{\mathbf{u}\otimes\mathbf{u}}$ is the Reynolds stress term.

Closure of (2) by calculation of $\rho\overline{\mathbf{u}\otimes\mathbf{u}}$ was achieved using the Shear Stress Transport model of Menter [7], which combined the ability of the $k\varepsilon$ model in modelling free stream turbulence with the ability of $k\omega$ in modelling flow near the wall, in a relatively inexpensive turbulence model. This model has been shown to predict separated flows well. Where the grid resolution was insufficient to implement the $k\omega$ model, wall functions were applied based on the approach of Ref. [8].

A finite-volume coupled solver was used to solve the equations on an unstructured hexahedral mesh. The coupled solver used an Incomplete Lower Upper (ILU) factorisation technique, combined with an algebraic multigrid technique [9] to accelerate convergence, and Rhie–Chow interpolation [10] to solve pressure and velocity on a co-located mesh.

Temporal discretisation was achieved using second-order backward-Euler time differencing with fixed time steps of $1 \times 10^{-5}$ s. Spatial discretisation of the advection terms used a second order scheme based on [11]. Each time step converged mass and momentum to more than 0.1% based on maximum residuals.

### 2.1. Model geometry and boundary conditions

The burner was based on the 1/30th scale isothermal physical models of burners in the stage II boilers at Yallourn W from Ref [5], Fig. 1. This 1/30th scale was chosen in order to get detailed information on both mean velocity and turbulent fluctuating components in near and far region of jets as presented by Yan and Perry [12,13]. The burner comprised a nearly square primary jet nozzle flanked above and below by rectangular secondary jet nozzles. The jets first discharged into a small recess in the main wall and then into a large open space. The walls of the recess were divergent at an angle of 10° and the geometric axis of the jets made an angle of 60° with the boiler wall. A small step was placed between the nozzles and the sidewalls of the recess. Geometrically similar jets exhibit similar hydrodynamic behaviour at Reynolds numbers above $1 \times 10^4$. Reynolds number is the product of hydraulic diameter of the jet, gas velocity and density over the viscosity of the fluid. Reynolds number in both the furnace and model burners was above $1 \times 10^5$; therefore, this model is expected to accurately reproduce the near-field development characteristics of burner-jets in a real furnace [14]. A comparison between the aerodynamic properties of jets in the physical model and the real furnace is shown in Table 1. The dimensions of the cross section of the primary jet and the secondary jet are given in Table 1. The hydraulic diameter ($D$), which is the diameter of a round nozzle with the equivalent cross-sectional area to the primary nozzle, is 0.0327 m.

For each jet the physical model used a section of ducting, which extended 50 hydraulic diameters (1.65 m) upstream from the nozzle and was fed from a plenum chamber, to achieve a developed flow at the nozzle. The CFD model assumed the jets discharged from a wall into a large open space, with Dirichlet constant pressure boundary conditions used at the open boundaries. These were placed far away from the jet itself, approximately 30 hydraulic diameters in the stream-wise direction, and 15 diameters in the cross-stream directions. Using a symmetry boundary condition on the primary jet centre plane halved the computational burden; the validity of this assumption was confirmed by performing one simulation of the full domain, which showed that no difference existed. Dirichlet boundary conditions were set on the inlet for all jets by specifying a flat velocity profile and turbulence quantities were set based on 1% turbulence intensity, which is appropriate for a flow coming from a plenum chamber. In furnace operation the momentum ratio between the secondary and primary jets

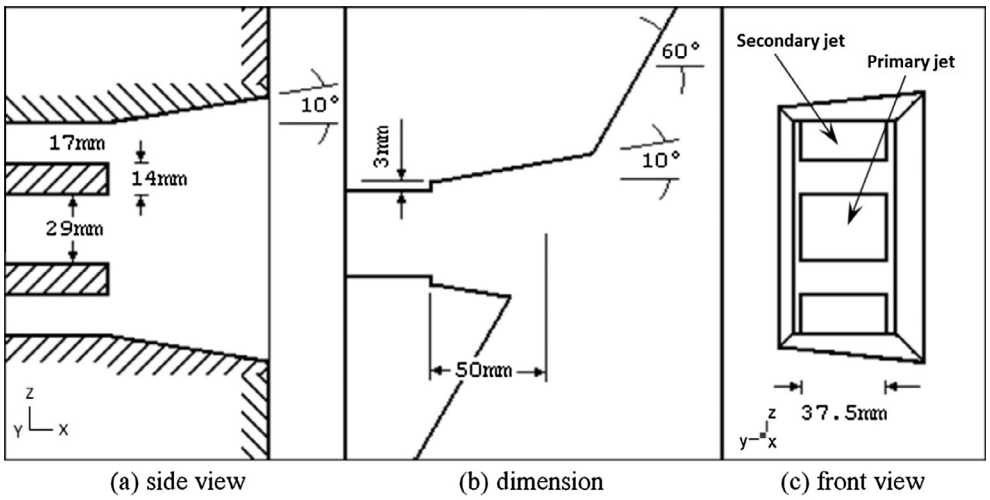


**Figure 1** Schematic diagram of the recessed burner.

**Table 1** Comparison of Yallourn and physical/CFD model nozzles.

| Property | Yallourn nozzle | | Model nozzle | |
|---|---|---|---|---|
| | Primary jet | Secondary jet | Primary jet | Secondary jet |
| Reynolds number | $4.6 \times 10^5$ | $3.8 \times 10^5$ | $1.3 \times 10^5$ | $9.3 \times 10^4$ |
| Slot width | 1020 mm | 1020 mm | 37.5 mm | 37.5 mm |
| Height | 800 mm | 565 mm | 29.0 mm | 17.0 mm |
| Gas velocity | 39.2 m $s^{-1}$ | 32.5 m $s^{-1}$ | 60 m $s^{-1}$ | 60 m $s^{-1}$ |
| *Base between jets* | | | | |
| Base height | 1020 mm | | 37.5 mm | |
| Width | 380 mm | | 14.0 mm | |

can vary. For the constant density flow modelled here this was achieved by using four secondary to primary jet velocity ratios, $\lambda = 1$, 1.4, 2.3 and 3, where the secondary jet velocity was held constant at 60 m/s and the primary jet velocity was reduced from 60 m/s to 40 m/s, 26 m/s and then 20 m/s.

### 2.2. Grids and grid dependence

The computational mesh was constructed using a body-fitted coordinate system and a hexahedral mesh, which mapped the geometrical features of the domain. A high-density mesh was used in the duct and jet cross sections and in the recessed cavity. Away from the jet an expansion factor was applied to the grid spacing in the cross-stream directions where the velocity gradients were small. In the stream-wise direction the grid was also coarsened from the nozzle onwards, although the coarsening was not as rapid, to ensure the entire length of the jet was captured with adequate resolution.

A grid dependence study was performed on a similar burner without a recess [15,1,2]. The tests were performed using the standard $k$–$e$ turbulence model with an upwind differencing scheme. Four grid refinements were performed, setting $4 \times 4$ cells in the primary duct cross section with similar grid distribution everywhere else, and then successively doubling the number of cells in the duct cross sections to $8 \times 8$ in the primary, then $16 \times 16$ and finally $32 \times 32$, with appropriate refinement elsewhere. Velocity profiles for each grid are compared in the xy plane and xz plane at a distance of 9D downstream of the jet nozzle which is the farthest point from the nozzle for which experimental data are available. Subsequent comparisons between the simulations and experiment were mainly carried out at this location making it most appropriate location to judge the grid dependence. Velocities were normalised to the centreline exit velocity of the primary jet. Change in the profiles was found with each successive grid refinement. The finer grids tended to predict less diffusive jets with higher centreline velocity. The grid density used for this recessed burner was more than double that was used for non-recessed burners, in an attempt to resolve the small features of the geometry. Therefore the results obtained from these simulations can reasonably be expected to be independent of the grid.

## 3. Results and discussion

Flow patterns in the recess were complex, caused by a combination of the internal reorganization of energy in the jet, adverse pressure gradients in the recess and entrainment of fluid into the jets. Pulsing was reported in [5] in the primary jet at $\lambda = 3.0$ and unsteadiness in the secondary jets at $\lambda = 1.0$. In the following sections the results of the CFD model are verified against the experimental measurements, followed by an exposition of the underlying vortex-shedding phenomenon responsible for the unsteady behaviour.

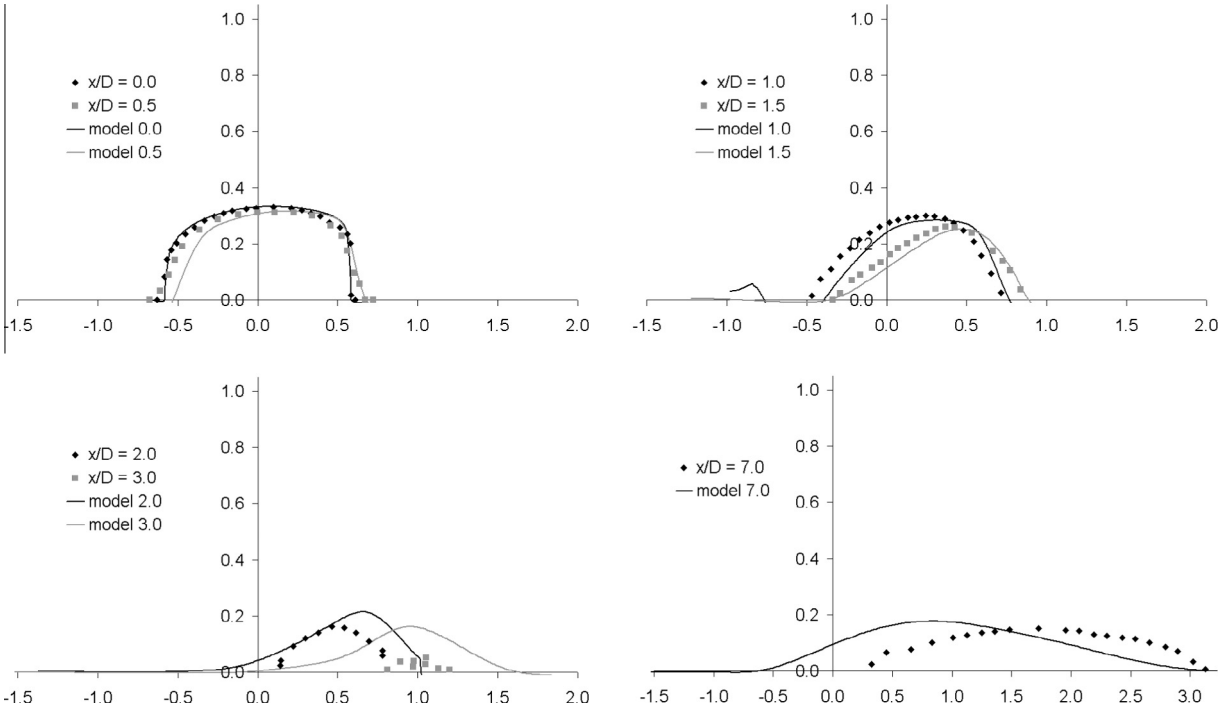


**Figure 2** Velocity profiles in the horizontal ($xy$) centre planes through the primary jets for $\lambda = 3$.

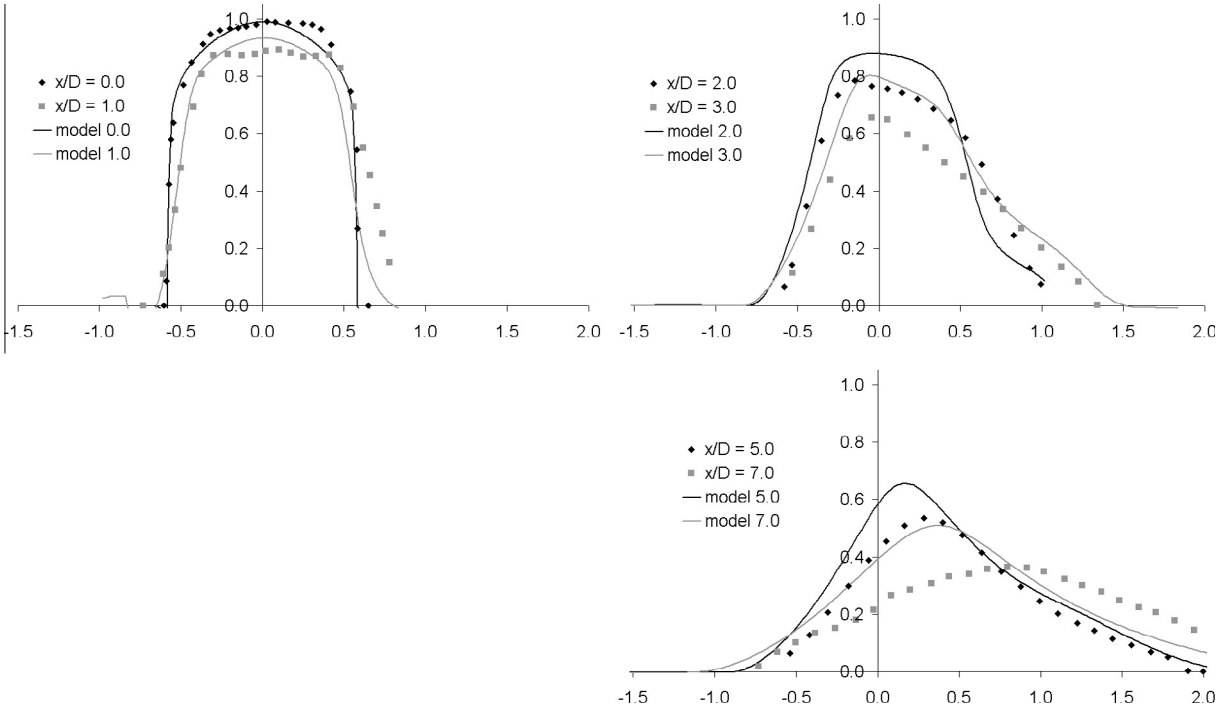


**Figure 3** Velocity profiles in the horizontal ($xy$) centre planes through the secondary jets for $\lambda = 3$.

### *3.1. Verification of velocity and pressure field predictions*

Velocity profiles in the horizontal ($xy$) centre planes through the primary and secondary jets and through the base region between the jets are shown in Figs. 2–4 for the case $\lambda = 3$ and in Figs. 5 and 6 for $\lambda = 1$. The predicted velocities were averaged over the length of a long simulation and then compared with the Pitot tube velocities measured by [5], to establish the accuracy of the simulations. All velocities are normalised to the centreline exit velocity of the primary jet

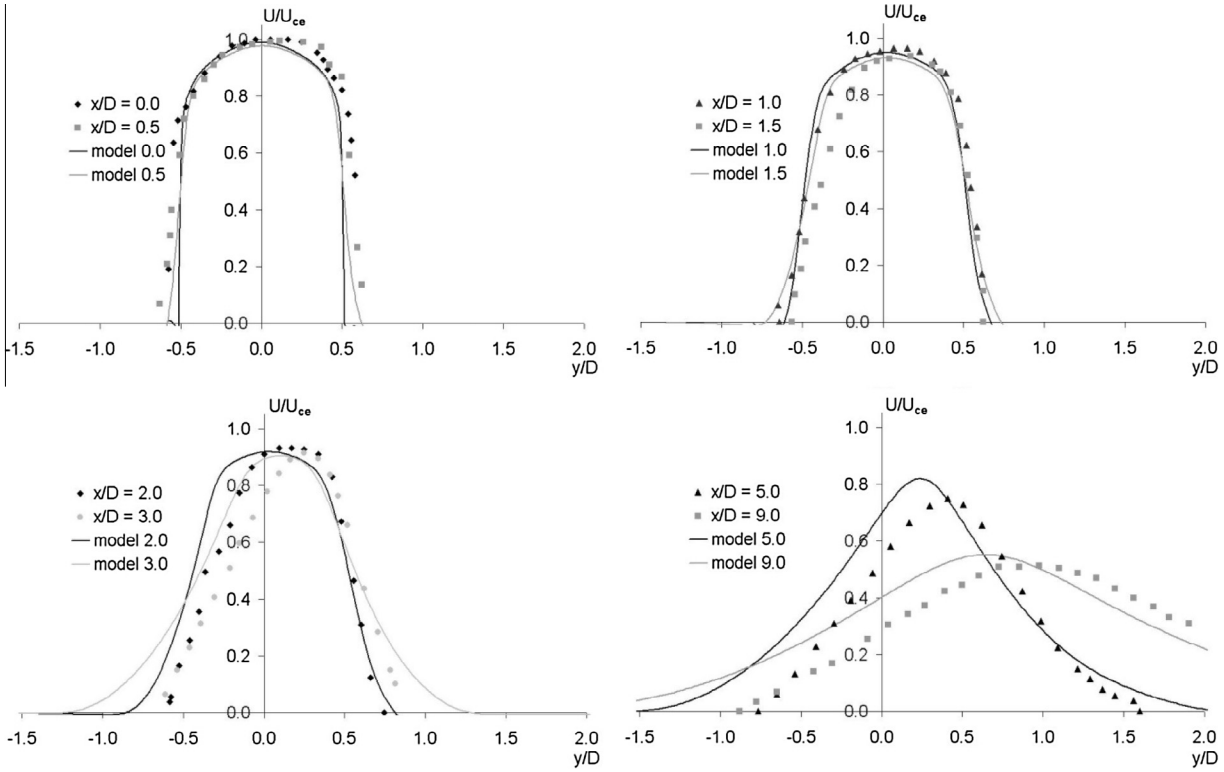


**Figure 4** Velocity profiles in the horizontal (*xy*) centre planes through the base region between the jets for $\lambda = 3$.

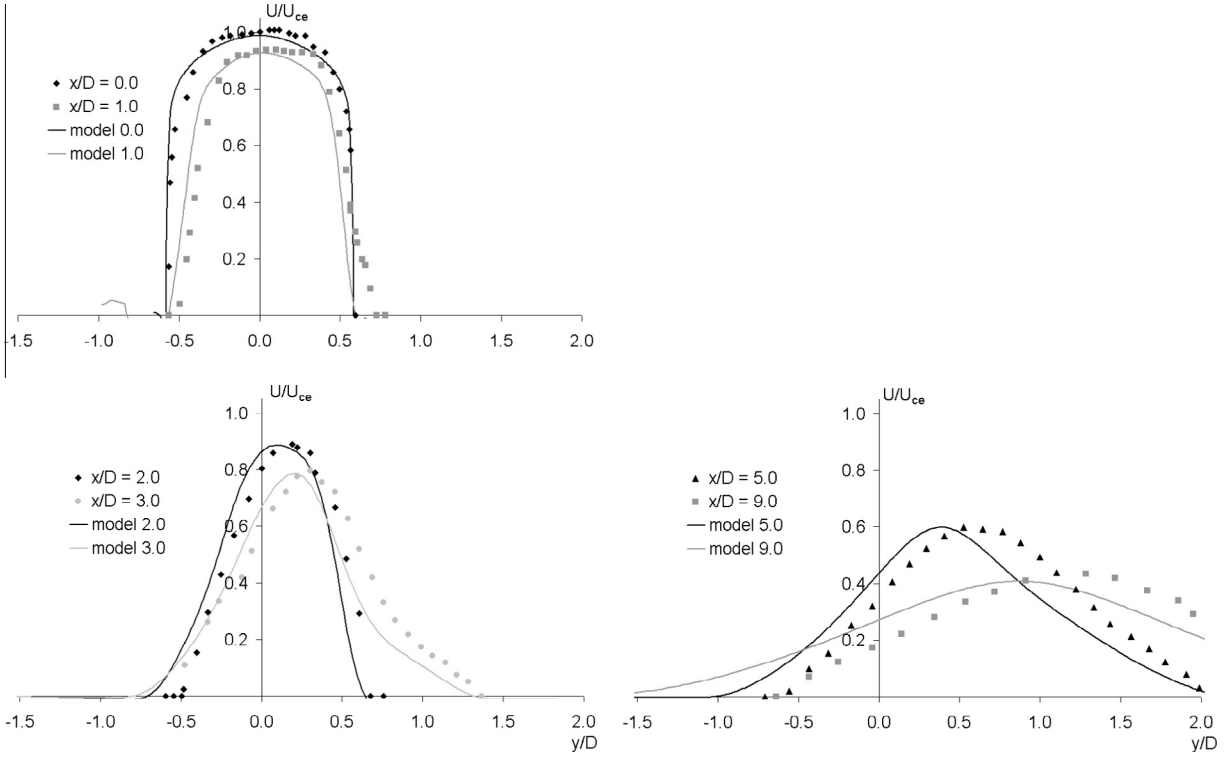


**Figure 5** Velocity profiles in the horizontal (*xy*) centre planes through the primary jets for $\lambda = 1$.

at $\lambda = 1$. Mean velocity profile predictions from a steady state model have already been published for $\lambda = 3$ [16], which were very similar to the transient results. The validity of using a steady state model to predict mean velocities is confirmed by

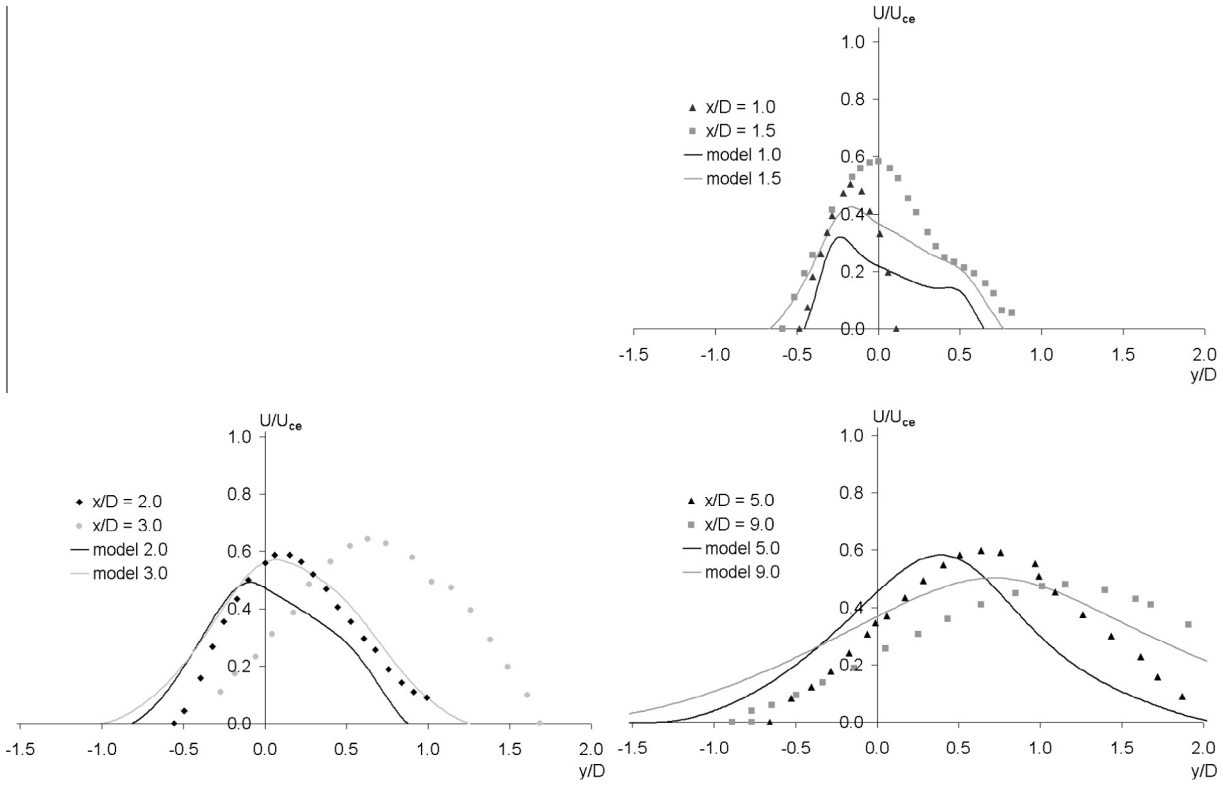


**Figure 6** Velocity profiles in the horizontal (*xy*) centre planes through the secondary jets for $\lambda = 1$.

this, and understood by the fact that while this flow is unsteady the timescale of the fluctuations was small, approaching the sort of timescales that would ordinarily be modelled by the turbulence model.

For the case where $\lambda = 3$, in the primary jet plane the CFD model generally predicted the same qualitative behaviour as observed in the physical jet, but there were some deficiencies in the quantitative accuracy of the model downstream of the recess. At the primary jet nozzle and at 0.5D, 1.0D and 1.5D the calculated profiles matched the measurements closely. Both jets clearly skewed away from their geometric axes towards the positive *y* side, or the long-wall of the recess. At 2.0D and 3.0D the jets continued to move from their geometric axes and dissipated quite quickly, the physical model having almost completely disappeared by 3.0D. The degree of velocity decay in the physical model was greater, although at velocities as low as this the accuracy of Pitot tube measurements would be substantially reduced. At 9.0D the primary jet had completely disappeared and the secondary jet had spread to the symmetry plane. The detailed explanation of the velocity decay of primary and secondary jet has been presented in [17]. The jets were similar in size and strength, but the CFD model jet did not deviate as far.

The velocity profile at the nozzle of the secondary jet was flatter in the physical model than the CFD model. At 1.0D the spread of the physical jet to the positive *y* side was more substantial, indicating a stronger attachment of the jet to the long wall. Between 2.0D at the end of the recess and 3.0D outside the recess the profiles tended to form strong peaks on the negative *y* side of the recess, or the short-wall side. These peaks appeared to be associated with a weak pulsation of the secondary jet velocity, which seemed connected with the vortex shedding in the primary jet. The profiles were very wide on the long-wall side; however, this was not only secondary jet flow because the primary jet was actually entrained along the recess wall and into the secondary jet. At 5.0D and 9.0D the comparison is generally good, except that the physical model jet decayed more rapidly and deviated more from its geometric axis than the CFD model predicted.

For the $\lambda = 1$ case, in the primary jet plane the CFD model generally predicted the same qualitative behaviour as observed in the physical jet, but there were some deficiencies in the quantitative accuracy of the model. At the primary jet nozzle and at 0.5D, the calculated profile was fairly symmetric about the centreline, but the measured profile was skewed towards the positive *y* side, or the long-wall of the recess. At 1D the CFD model predicted the jet boundary well. At 1.5D the prediction on the long-wall side was good but on the short-wall side, where the jet was exposed to the open atmosphere outside the recess, the velocity gradient was too steep and the jet was too wide. Little change occurred by 2D. At 3D the jets had exited the recess and were free jets; the differences in the profiles were similar to the previous two locations, but it is clear that the deviation of the jet from the geometric axis of the burner was less in the simulations. At 5D and 9D the CFD model was generally similar to the physical model but it tended to predict a slightly higher velocity decay rate and less deviation from the geometric axis.

The secondary jet velocity profiles matched the physical measurements better than the primary jet profiles, especially in the region just outside the recess. At the nozzle and at 1D and 2D the CFD model matched the experimental profile clo-

sely. The size and shape of the profiles at 3D, 5D and 9D were essentially the same for the simulation and physical model, but there was less movement of the jet off its geometric axis in the simulation.

The spacing between the nozzles, or the base region, provided a path for air to be entrained into the jets. In this plane between the jets the velocity profiles inside the recess were somewhat different in the simulation than in the physical model, although both showed that significantly higher entrainment occurred on the short side, because that side was more open to the outside atmosphere and the entrainment path was easier. On the long side the physical model showed zero velocity at 1D, indicating that the entrained flow did not reach the back part of the recess on that side. There was a major discrepancy at 3D, but considering that for the physical model the centre of the profiles for the primary and secondary jets in Figs. 5 and 6 was at about $y = 0.3$D and for the base region it was $y = 0.7$D, and there appeared to be some inconsistencies in the physical measurements. The level of agreement between the simulation and the physical model in the plane of the base region was at about the same level as for the other profiles. In general, the simulations tended to predict the correct behaviour, but the deviation of the jets from their geometric axes was slightly less than in the physical model.

The mean static-pressure distribution on the walls of the recess is shown in Fig. 7 and a comparison of the pressure tapings at the points indicated in the figure is presented in Fig. 8. There were discrepancies between the physical measurements and the simulation, the most notable being the much higher pressures in the physical model towards the opening of the recess and along the long-wall side of the recess, especially in the centre plane of the primary jet. There was potential for large errors in the experimental data presented here, due firstly to difficulties in reading the original data from the figures in [5] and also due to the oscillation of the pressure readings in the measurements themselves, which could have been affected by the dynamic response of the pressure tubes [18]. However, even the authors of [5] only drew general conclusions from these measurements, namely that the pressure distribution on the base between the jets was concave, that is a lower pressure in the middle, and that there was a large adverse pressure gradient along the diverging walls of the recess and the pressure distribution was asymmetric across the recess. The same observations were made with the simulation results.

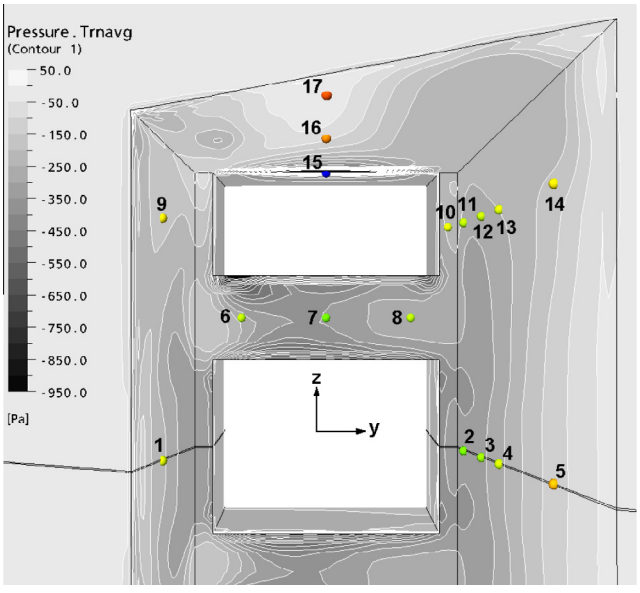


**Figure 7** The mean static-pressure distribution on the walls of the recess burner.

### 3.2. Flow field development

Because of its divergent walls the recess acted to some extent like a diffuser, whether or not that was originally the intention is unknown. The idea of an efficient diffuser, as described by [19], was to recover kinetic energy from the mean flow in the form of a rise in pressure, by expanding the duct smoothly to prevent separation of the flow from the walls. The pressure in the diffuser is higher in the centre than on the walls, and this pressure difference results in a force being applied perpendicular to the streamlines and directed outwards from the centre, which helps bend the streamlines to follow the diverging walls. An inefficient diffuser is one in which the flow separates as it moves into diverging section, preventing adequate expansion and deceleration of the flow to give the required pressure rise.

Full or partial separation often occurred in this burner geometry, which was aided by the large expansion angle of 10° and the presence of the small step after the nozzle. The other peculiarity of this geometry was its angled opening, which resulted in an asymmetric pressure distribution in the recess and a cross-stream pressure drop. The pressure just upstream of the nozzle tended to be uniform across the ducts, but in the recess the pressure would naturally tend to equalise with the atmospheric pressure across the opening, which was angled at 30° to the nozzles. Additionally, the jets tended to entrain fluid immediately upon leaving the nozzle but the entrainment path was longer and more difficult on the long-wall side than the short-wall side, which tended to establish a lower pressure on the long-wall side near the nozzle. The pressure distribution on the symmetry plane of the recess is shown in Fig. 9 for $\lambda = 3$.

The cross-stream pressure drop favoured the bending of streamlines towards the long wall side and the results of this are clearly seen in the velocity profiles. The movement of the jets from their axes was far more pronounced at lower velocities; the primary jet deflected by 30° for $\lambda = 3$ and by only 8° for $\lambda = 1$. The larger deflection occurred because the reduced momentum was unable to overcome the force exerted by the pressure gradient and the jet was pushed towards the long wall.

Another result of the peculiar pressure distribution was vortex shedding in the jets, which was so severe at $\lambda = 3$ that it was described in [5] as jet pulsing. The curious nature of this phenomenon was that the vortices were only present in either the primary jet (at $\lambda = 3.0$ and 2.3) or the secondary jets (at $\lambda = 1.4$ and 1.0), depending on the velocity ratio, but never in both at the same time. Evidence of vortices is seen in the local low-pressure region on the short-wall side in Fig. 9, which resulted from the continual passage of low-pressure vortex cores.

Discussing their observations of this primary jet pulsation in their physical model the authors of [5] commented that

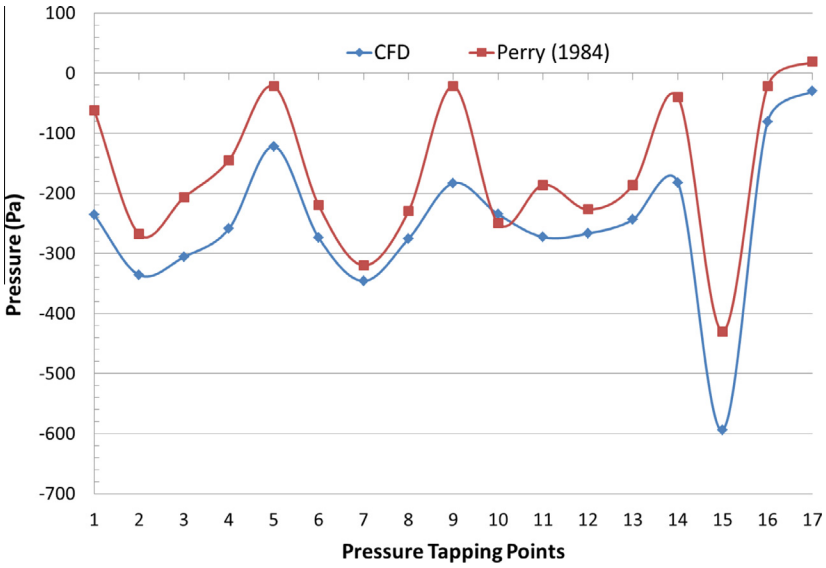


**Figure 8** Comparison of the pressure tapings at reference points.

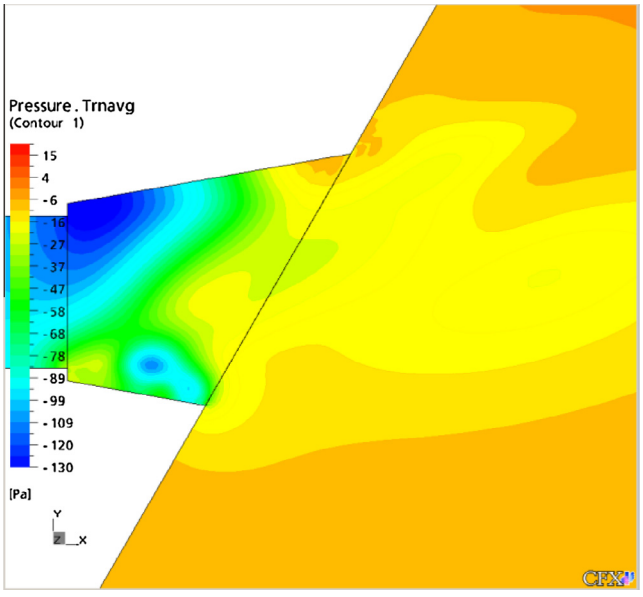


**Figure 9** The pressure distribution on the symmetry plane of the recess for $\lambda = 3$.

the physical mechanism producing this behaviour might be related to the 'whistler nozzle' first discovered by [16], based on similarities in the geometry and overall effect. The whistler nozzle phenomenon occurs when a short expansion collar is fitted to a circular pipe nozzle, producing excitation at discrete frequencies for certain combinations of velocity, duct length, collar length and collar to duct diameter ratio.

It was shown by [18] that the phenomenon was caused by the coupling of three resonant mechanisms, the shear layer tone, the organ-pipe resonance of the nozzle and the 'preferred mode' of the jet, all of which must occur simultaneously to produce the excitation. That the vortex shedding in the recess occurred at two different velocities for the same geometric configuration indicated that the same coupling was not required for this nozzle to produce the excitation. The shear layer impinged on the recess lip on the long-wall side at $\lambda = 3.0$ in a fashion that might be expected to produce a shear layer tone [19], but impingement did not occur at $\lambda = 2.3$, precluding this from being the excitation mechanism.

The frequency of vortex shedding was 130 Hz at $\lambda = 3.0$ and 170 Hz at $\lambda = 2.3$, which corresponded to a Strouhl number of 0.42 which is ratio of the product of frequency of vortex shedding and hydraulic diameter of the jet over the jet velocity. When the vortex shedding shifted to the secondary jets the frequency changed again, 280 Hz for $\lambda = 1.4$ and 400 Hz for $\lambda = 1.0$, but the Strouhl number remained at 0.42, which is within the range of preferred rectangular jet frequencies reported in the literature [20], although those frequencies were for isolated jets. This indicates that it was the recess resonance that enabled the jets to oscillate in their preferred modes [19].

Fig. 10 shows a time sequence covering one full period of oscillation in the primary jet at $\lambda = 3$. The symmetry plane was seeded with streamlines from the primary jet (grey) and also from locations near the opening where outside air was entrained into the recess (black). A large vortex formed in the shear layer on the short-wall side behind the high-pressure region at the opening of the recess, where the adverse pressure gradient was large enough to block the low-momentum jet and turn it back towards the wall. This fluid was then re-entrained back into the jet forming the vortex. The recirculation grew in size returning more fluid to the jet and increasing its momentum sufficiently to overcome the adverse pressure gradient, at which point the vortex shed and was convected out of the recess. The sequence also shows the impingement of the jet onto the lip of the recess on the long-wall side.

As $\lambda$ was reduced to 2.3 the vortex became smaller because the primary jet had more momentum and less returned fluid was required in order to overcome the adverse pressure gradient, Fig. 11. The increased momentum also prevented the cross-stream pressure gradient from pushing the jet as far off the geometric axis and it no longer attached to the lip of the

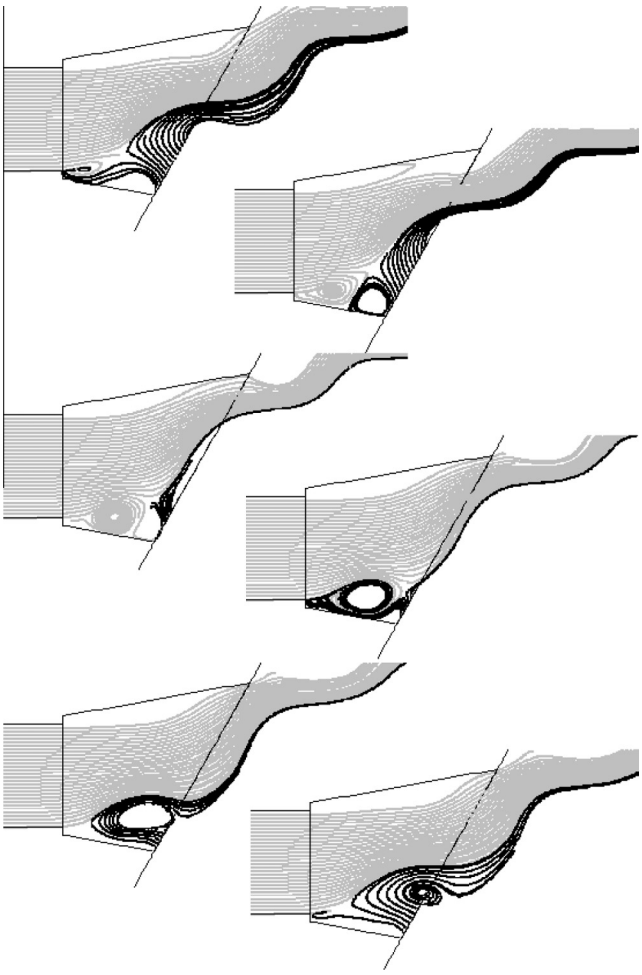

**Figure 10** Time sequence covering one full period of oscillation in the primary jet at $\lambda = 3$.

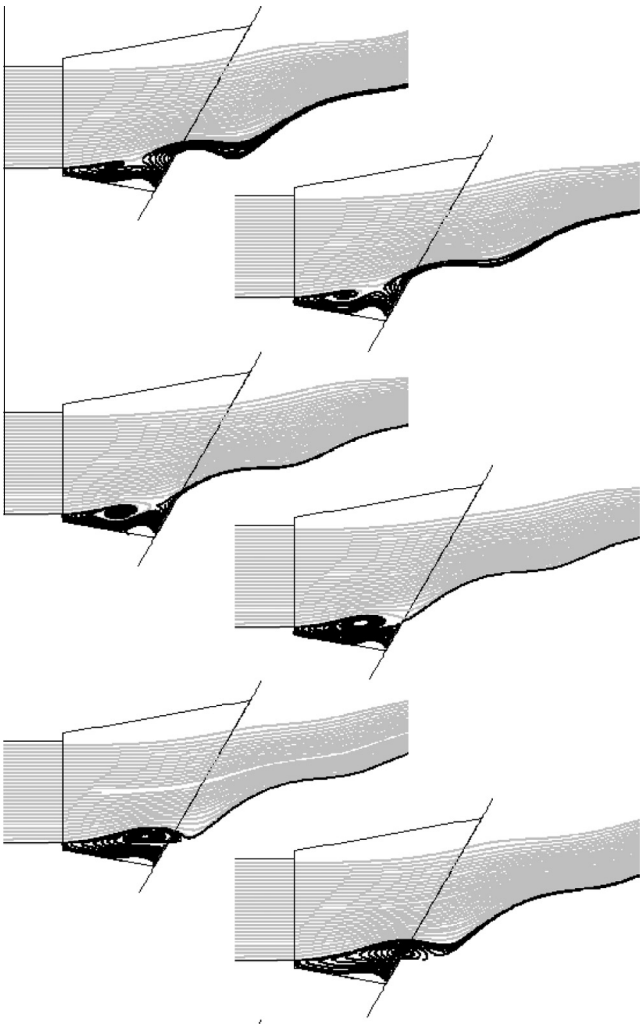

**Figure 11** Time sequence covering one full period of oscillation in the primary jet at $\lambda = 2.3$.

recess on the long-wall side. At $\lambda = 1.4$ the vortex was smaller again and no longer shed out of the recess, but became stationary and at $\lambda = 1.0$ the vortex had all but disappeared from the primary jet.

A two-dimensional simulation of the recess cross section is unable to reproduce the vortices at any velocity. At the lowest velocity the adverse/cross-stream pressure gradient caused the jet to attach to the long-wall as soon as it left the duct, turning the jet strongly away from its geometric axis and leaving the recess very open on the short side, allowing a steady flow of entrained fluid to easily enter the recess. This indicates the truly three-dimensional nature of the vortex shedding.

It was the combination of low jet momentum, the adverse pressure gradient and the entrainment into the base region between the primary and secondary jets that triggered the unsteadiness and allowed the vortices to form. While the jets were free to entrain fluid upon leaving the nozzles, replacement of this fluid from outside was difficult because the recess was only partially open to the ambient surroundings. The static pressure in the base region became very low in order to facilitate its replacement, seen in Figs. 7 and 8 for $\lambda = 1$. At lower velocities, the combination of this low static pressure in the base region and the pressure blockage of the adverse pressure gradient near the opening of the recess were sufficient to draw some of the short-wall side shear layer of the primary jet back up into the base region, initiating the reverse flow and the vortex, Fig. 12.

This flow field bears some similarities to that used by [21] to initiate global instabilities in a flow over a backward facing step. They induced self-excited oscillations by applying suction to the step face, which is analogous to the suction effect of the base region entrainment, and blowing at the wall adjacent to the step, which is similar to the flow of entrained ambient fluid into the recess. With the goal of global flow destabilisation, their use of suction was motivated by the fact that it increases local absolute growth rates in free shear flows, whereas the blowing was aimed at reducing nonparallelism, i.e. spatial evolution of the flow. In this case the suction of the base region clearly increased the local absolute growth rate of the instability in the primary jet. While the two-dimensional backward facing step required external forcing to convert the stationary

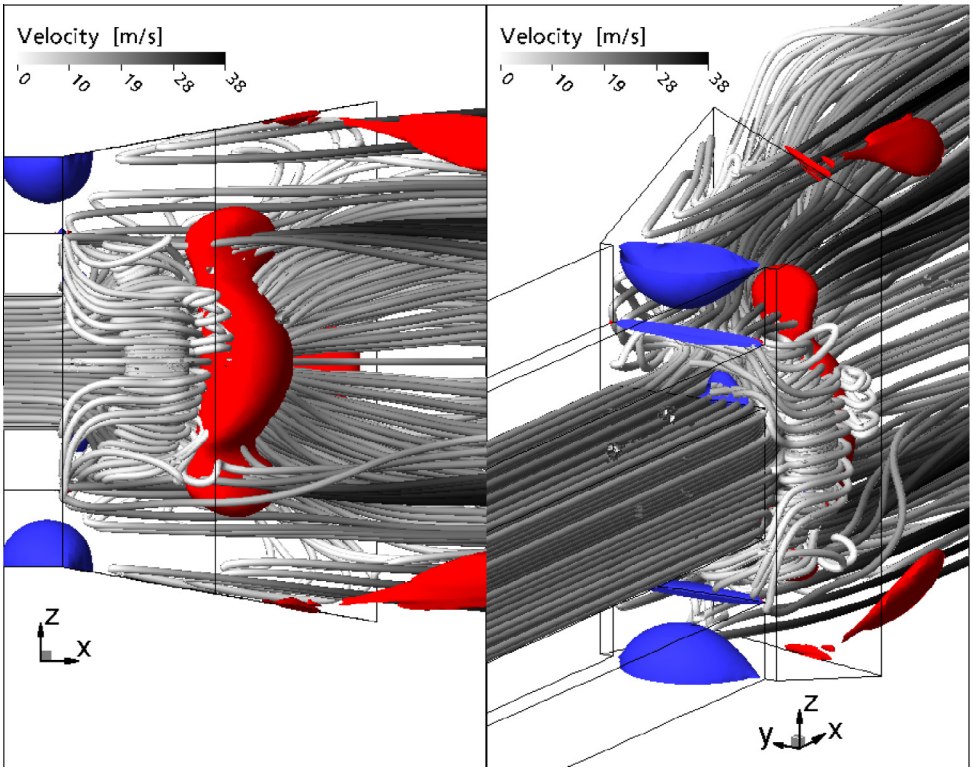


**Figure 12** Entrainment into base region between the jets and its role in development of vortices.

vortex into a convective instability, the complex geometry and flow field of the jets in the recess provided a naturally occurring means of generating the shear layer instability and making it globally unstable.

Fig. 13 illustrates how the adverse pressure gradient changed with increasing $\lambda$. The graphs show the static pressure in the recess along a line on the short side of the recess, beginning at the nozzle and ending just outside the recess and lying on the symmetry plane of the primary jet. Each graph contains six lines, which were the pressure distribution at 6 time steps covering one full period of vortex shedding. The topmost graph shows the pressure rise experienced under the conditions of $\lambda = 1$. The low pressure at the nozzle of $-500$ Pa was risen slowly until mid-recess, where the pressure gradient sharply increased until close to the mouth of the recess. The pressure was fairly constant at the nozzle but at the mouth there was a significant amount of fluctuations in the pressure due to vortex shedding in the secondary jet. At $\lambda = 1.4$ the nozzle pressure was only $-300$ Pa, but the shape of the curves was similar to $\lambda = 1.0$ with a higher gradient in the middle of the recess, and there was also less fluctuation in the pressure at the mouth due to the reduction in strength of secondary jet vortex shedding at this velocity ratio. At $\lambda = 2.3$ the nozzle pressure was still around $-300$ Pa but there was a sharp pressure rise close to the nozzle and after about one third of the way out of the recess it became fairly constant, with some small fluctuations due to the small amount of vortex shedding in the primary jet. At $\lambda = 3.0$ the nozzle pressure was still only $-300$ Pa and the sharp pressure rise occurred in about the same location at $\lambda = 2.3$, but there were large fluctuations in pressure from about one third distance due to the large amount of vortex shedding that occurred at this velocity ratio.

At higher $\lambda$ the secondary jet was able to fulfil its entrainment requirements easily; from the corner regions of the recess and from the base region, which was left more open for entrainment from the outside because of the reduced flow coming from the primary jet, and also by entrainment of the lower momentum primary jet itself. This allowed the secondary jet to operate quite stably at higher $\lambda$. As $\lambda$ was reduced and the primary jet velocity increased, it became more difficult for the secondary jet and the entrainment into the relatively open top corners of the recess increased to compensate, significantly increasing the shear in this region. This increased shear, in combination with the very large adverse pressure gradient, resulted in vortices forming on either side of the secondary jet in a manner similar to the primary jet vortices.

The adverse pressure gradient was larger in secondary jets because of two factors; firstly jets underwent an initial reduction in pressure because of their acceleration around the small corner that formed the join between the ducts and the top and bottom walls of the recess, and secondly the expansion of the top and bottom walls meant that more pressure was recovered than in the primary jet. A comparison of the pressure gradients along the top and side walls can be made from Figs. 7 and 8, where the wall static pressure at the join relative to the ambient atmosphere is seen to be more than $-1$ kPa. When a small step was placed between the ducts and the expanded top and bottom walls, similar to that in the sidewalls, the jets completely separated from the top and bottom walls and the vortex shedding disappeared.

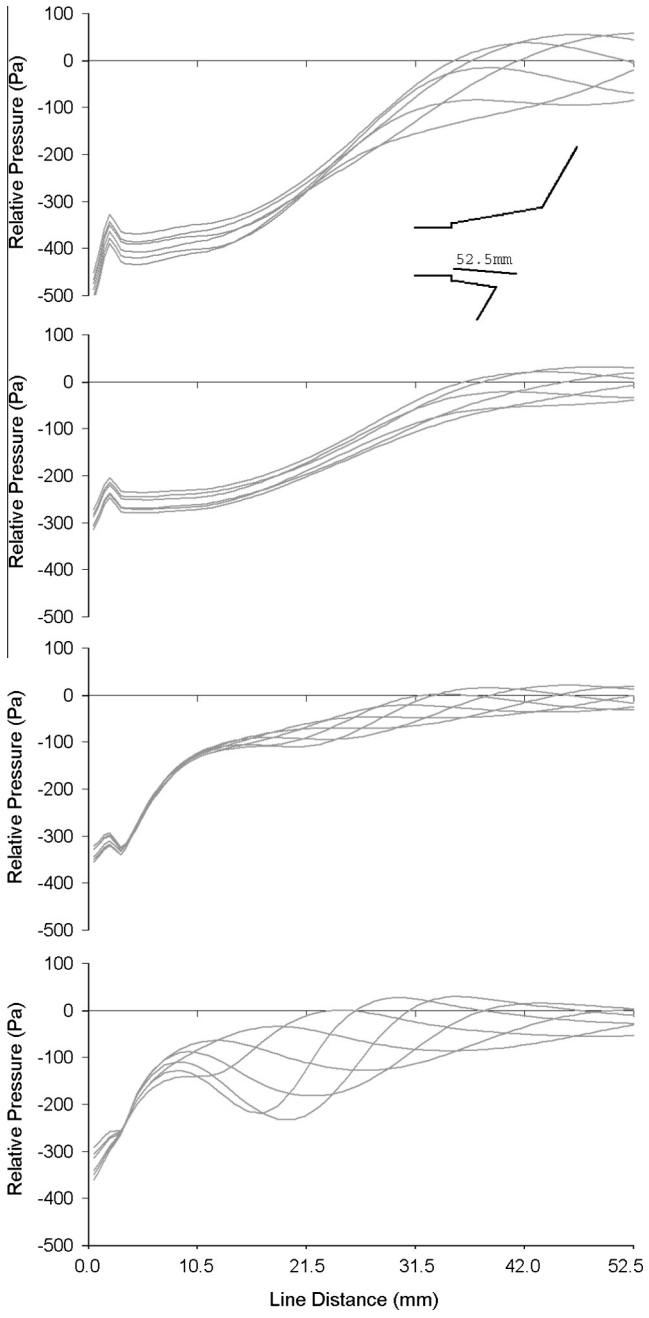


**Figure 13** Effect of the adverse pressure gradient changed with increasing $\lambda$.

## 4. Conclusion

The asymmetric expansion of the recess resulted in two dramatic changes in jet behaviour, movement of the jets away from their geometric axes and vortex shedding within the jet. The amount of movement, between 8° and 30°, has two main implications for burner operation; firstly the jets may no longer be correctly aimed at the swirling fireball in the centre of the furnace and the fuel delivery may be affected and secondly, at the higher velocity ratio the primary jet moved out of alignment with the secondary jets, preventing adequate mixing of the fuel and air streams and potentially resulting in incomplete combustion. The former is mainly of concern in existing furnaces if this movement was not accounted for when locating the burner in the furnace wall, but is of less concern when designing a new boiler. The latter is of concern in both cases because it is not easy to correct without modification to the burner design.

Vortex shedding is not necessarily detrimental to the burner operation, except for example by causing vibration-induced fatigue, and it may even be desirable for improved mixing. The vortex shedding initiated in this burner would undoubtedly accelerate mixing of the jets with the hot combustion gases in the furnace, which would heat the fuel mixture more rapidly. Vortices in the primary jet were only found on one side of the recess, the short side, which may not allow uniform heating of the jet. There did not appear to be any large scale mixing of the primary jet with the secondary jets, at least in the near field. But increased turbulence may be beneficial further downstream, as long as the jets remain in the same vertical plane so that large-scale turbulent structures can enhance transport fluid between the two streams. The potential benefits could be determined using a passive tracer to model species transport in the jets.

An ideal scenario for burner operation would be making use of the adverse pressure gradient created by the expanded recess geometry to induce some large-scale vortices for enhanced mixing, while reducing the deviation of the jets from their geometric axes, at least to the extent that the primary and secondary jets remained in the same plane. It would also be desirable to continue to allow entrainment of ambient boiler fluid into the jets.

In the original physical model the primary duct was extended past the boiler wall, which prevented the movement of the jet from its geometric axis and removed the pulsation. The current study shows that the reason for this was because the extension of the duct put the nozzle beyond the adverse/cross-stream pressure gradient inside the recess; however, it also prevented the ambient fluid from being entrained into the primary jet inside the recess and also delayed the mixing of the primary and secondary jets.

## References

[1] J.T. Hart, J.A. Naser, P.J. Witt, Aerodynamics of an isolated slot-burner from a tangentially-fired boiler, Appl. Math. Model. 33 (9) (2009) 3756–3767, http://dx.doi.org/10.1016/j.apm.2008.12.020.

[2] A.A. Bhuiyan, M.R. Karim, J.Y. Hart, M. Rahman, J. Naser, Experimental and numerical investigation of coherent structure dynamics on mass transfer in a separated cavity flow, Exp. Therm. Fluid Sci. (2016).

[3] S. Ahmed, J. Hart, J. Nikolov, C. Solnordal, W. Yang, J. Naser, Investigation of aerodynamics of a recessed rectangular slot-burner used in tangentially-fired furnaces by varying jet velocity ratio in the presence of cross-flow, Exp. Therm. Fluid Sci. 68 (2015) 109–122.

[4] Z.F. Tian, P.J. Witt, W. Yang, M.P. Schwarz, Numerical simulation and validation of gas-particle rectangular jets in crossflow, Comput. Chem. Eng. 35 (4) (2011) 595–605, http://dx.doi.org/10.1016/j.compchemeng.2010.09.007.

[5] J. Perry, T. Hausler, Aerodynamics of burner jets designed for brown coal fired boilers-part IV. Final report for NERDDC Grant No. ND/84/004, 1984.
[6] J. Perry, Aerodynamics of burner jets designed for brown-coal fired boilers–Part I literature survey, in: SECV Engineering Research Division Report No, 1981.
[7] F.R. Menter, Two-equation eddy-viscosity turbulence models for engineering applications, AIAA J. 32 (8) (1994) 1598–1605.
[8] H. Grotjans, F. Menter, Wall functions for general application {CFD} codes, 1998.
[9] B. Hutchinson, G. Raithby, A multigrid method based on the additive correction strategy, Numer. Heat Transfer, Part A: Appl. 9 (5) (1986) 511–537.
[10] C.-M. Rhie, Numerical study of the flow past an isolated airfoil with separation, Diss. Abstr. Int. Part B: Sci. Eng. 42 (9) (1982).
[11] T.J. Barth, D.C. Jespersen, The design and application of upwind schemes on unstructured meshes, 1989.
[12] H. Yan, J.H. Perry, Two-phase flow development in slot-burners – Part 1 Flow visualization study, in: ESAA Report No. ES/93/01, 1994.
[13] H. Yan, J.H. Perry, Two-phase flow development in slot-burners – Part 2 detailed flow measurement and numerical model validation, in: ESAA Report No. ES/94/01, 1994.
[14] F. RIC0U, D. Spalding, Measurement of entrainment by axisymmetric turbulent jets, J. Fluid Mech. (1) (1961) 21–32.
[15] S. Ahmed, Aerodynamics of Rectangular Slot-Burners and Combustion in Tangentially-Fired Furnace, Swinburne University of Technology, Australia, 2005.
[16] W. Hill, P. Greene, Increased turbulent jet mixing rates obtained by self-excited acoustic oscillations, J. Fluids Eng. 99 (3) (1977) 520–525.
[17] S. Ahmed, J. Hart, J. Naser, The effect of jet velocity ratio on aerodynamics of rectangular slot burners in tangentially fired furnace, in: Paper Presented at the Third International Conference on CFD in the Minerals and Process Industries, Melbourne, Australia, 10–12 December 2003.
[18] A. Hussain, M. Hasan, The 'whistler-nozzle'phenomenon, J. Fluid Mech. 134 (1983) 431–458.
[19] A. Hussain, K. Zaman, The free shear layer tone phenomenon and probe interference, J. Fluid Mech. 87 (02) (1978) 349–383.
[20] F. Grinstein, Vorticity dynamics in spatially developing rectangular jets, in: AIAA, Shear Flow Conference, Orlando, FL, 1993, p. 1993.
[21] L. Kaiktsis, P.A. Monkewitz, Global destabilization of flow over a backward-facing step, Phys. Fluids (1994-present) 15 (12) (2003) 3647–3658.